

The N-terminal acetylation of α -synuclein slows down its aggregation process and alters the morphology of the resulting aggregates

Rosie Bell¹, Rebecca J. Thrush¹, Marta Castellana-Cruz¹, Marc Oeller¹, Roxine Staats¹,
Aishwarya Nene¹, Patrick Flagmeier¹, Catherine K. Xu¹, Sandeep Satapathy²,
Celine Galvagnion³, Mark R. Wilson⁴, Christopher M. Dobson¹, Janet R. Kumita^{5*} and
Michele Vendruscolo^{1*}

¹*Centre for Misfolding Diseases, Department of Chemistry,
University of Cambridge, Cambridge CB2 1EW, UK*

²*Blavantik Institute, Dept. of Cell Biology, Harvard Medical School, Boston, USA*

³*Department of Drug Design and Pharmacology, Faculty of Health and Medical Sciences,
University of Copenhagen, Copenhagen, Denmark*

⁴*School of Chemistry and Molecular Bioscience, Molecular Horizons Institute,
University of Wollongong, Australia*

⁵*Department of Pharmacology, University of Cambridge, Cambridge CB2 1PD, UK*

Abstract

Parkinson's disease is associated with the aberrant aggregation of α -synuclein. Although the causes of this process are still unclear, post-translational modifications of α -synuclein are likely to play a modulatory role. Since α -synuclein is constitutively N-terminally acetylated, we investigated how this post-translational modification alters the aggregation behaviour of this protein. By applying a three-pronged aggregation kinetics approach, we observed that N-terminal acetylation results in a reduced rate of lipid-induced aggregation and in a slowing down of both elongation and fibril-catalysed aggregate proliferation. An analysis of the amyloid fibrils produced by the aggregation process revealed different morphologies for the acetylated and non-acetylated forms in both lipid-induced aggregation and seed-induced aggregation assays. In addition, we found that fibrils formed by acetylated α -synuclein exhibit a lower β -sheet content. These findings indicate that N-terminal acetylation of α -synuclein alters its lipid-dependent aggregation behaviour, reduces its rate of *in vitro* aggregation, and affects the structural properties of its fibrillar aggregates.

Introduction

Parkinson's disease (PD) is the second most common neurodegenerative disorder, with over 6 million people worldwide suffering from this condition^{1,2}. Age is a major risk factor of PD, affecting about 1-2% of people over the age of 65, and 4% of people over the age of 85^{3,4}. PD is characterised by a loss of dopaminergic neurons from the *substantia nigra pars compacta* and by the presence of Lewy bodies and Lewy neurites in neurons, which are predominantly composed of aggregates of the 14 kDa intrinsically disordered protein, α -synuclein⁵ and lipid membranes⁶.

α -Synuclein was linked with PD when *SNCA*, the gene encoding α -synuclein, was found to be mutated in a subset of early-onset PD patients. Six mutations within the *SNCA* gene have been linked with PD (A53T/E, A30P, E46K, H50Q and G51D); *SNCA* duplication and triplication were also found to cause early onset familial PD⁷⁻¹⁴. The functions of α -synuclein involve the regulation of synaptic vesicles sorting, lipid transport and synaptic plasticity^{15,16}. In neurons, α -synuclein exists primarily as an intrinsically disordered monomer, and as a membrane-bound α -helical state^{15,16}. Upon dysregulation, α -synuclein can aggregate to form cross- β amyloid fibrils, via less organised oligomeric intermediates (**Figure 1**)¹⁷, which appear to be particularly neurotoxic^{18,19}.

α -Synuclein is subject to multiple post-translational modifications, including N-terminal acetylation^{20,21}. Cytosolic and pathologically deposited α -synuclein from dementia with Lewy-bodies (DLB) and PD patients, from post-mortem hippocampal, temporal, cingulate, and prefrontal cortical grey matter regions, was analysed by tryptic digestion and liquid chromatography with tandem mass spectrometry (LC-MS/MS), to show that this α -synuclein is constitutively N-terminally acetylated²². N-terminal acetylation is a common post-translational modification carried out in eukaryotes by N-terminal acetyltransferases (Nat) and 85% of eukaryotic proteins are N-terminally acetylated²³. To allow for N-terminal acetylation to be introduced in *E. coli*, a pNAT system was developed for the co-expression of a yeast Nat enzyme with the protein of interest^{24,25}. The addition of an acetyl group to the amine group at the N-terminus results in the loss of a positive charge (**Figure 2**). This change is relevant to the intrinsically disordered monomeric state of α -synuclein, where there are interactions between the negative C-terminal region and positive N-terminal region^{26,27}. Furthermore, the N-

terminus is in a region of poor solubility²⁸ and disrupting the charge or electrostatic interactions may change the biophysical properties of α -synuclein.

In this work we assessed the effects of N-terminal acetylation on the *in vitro* aggregation of α -synuclein. We used three conditions, each favouring different individual microscopic processes in the overall aggregation reaction (lipid-induced aggregation, surface-catalysed fibril amplification and fibril elongation) to investigate how N-terminal acetylation affected each of these microscopic steps. For each of these conditions, we found that N-terminal acetylation decreased the rate of aggregation. Previous studies have shown that N-terminal acetylation reduces the rate of α -synuclein aggregation in the presence of sodium dodecyl sulfate (SDS) micelles²⁹ in non-quiescent conditions³⁰ and decreases oligomerisation rates in unseeded quiescent conditions³¹. Other studies reported that N-terminal acetylation increases α -helicity in the N-terminus of α -synuclein and increases its affinity for lipid vesicles^{32–37}. The effects of N-terminal acetylation on the morphology of α -synuclein fibrils has also been studied with varying results. N-terminally acetylated α -synuclein and unmodified α -synuclein have been reported as morphologically indistinct³², or to exhibit differences in fibril periodicity and length³⁸. The stability of both acetylated α -synuclein and unmodified α -synuclein fibrils was reported to be similar in denaturant, but with unmodified α -synuclein being more resistant to protease cleavage³⁸.

Under the conditions used in previous studies, it is likely that all microscopic stages of aggregation occur (nucleation, elongation, surface-catalysed fibril amplification, **Figure 1**). In this study we built on the observation that it is possible to alter the solution conditions to favour the different process of aggregation³⁹. In separating out the stages of aggregation we can gather more information on the transient aggregation intermediates such as oligomers and protofibrils^{40,41}. Given that α -synuclein is constitutively N-terminally acetylated, we used this approach to investigate how this post-translational modification affects the process of amyloid aggregation, fibril formation, morphology and stability, particularly as α -synuclein fibrils catalyse the formation of oligomers by surface-catalysed fibril amplification⁴².

Results

N-terminal acetylation does not significantly alter the conformational properties of monomeric α -synuclein

To compare the behaviour of N-terminal acetylated and non-acetylated α -synuclein in its monomeric form, the secondary structure was analysed by circular dichroism (CD) spectroscopy (see Methods). Both forms of α -synuclein monomers had highly disordered structures as expected (**Figure 3A**).

Since the ability of α -synuclein to bind to lipid membranes plays an important function role^{16,43}, and lipid membranes may promote α -synuclein aggregation and lead to the presence of lipids in Lewy bodies⁶, we analysed the binding of monomeric α -synuclein to vesicles of dimyristoyl phosphatidylserine (DMPS), which have been previously shown to induce the aggregation of α -synuclein⁴¹. The binding of α -synuclein to DMPS vesicles was measured by CD spectroscopy (see Methods). We observed slightly less α -helical secondary structure in the protein upon DMPS addition for acetylated α -synuclein (**Figure 3C,D**). The α -helical content of the N-terminus of the monomeric vesicle bound form of acetylated α -synuclein was reported to increase when bound to SDS vesicles, suggesting that the conformational properties of α -synuclein depend on the composition of the lipid membranes. The change in mean residue ellipticity at 222 nm, which reports on the α -helical content, did not show a statistically significant difference in the ability of acetylated and non-acetylated α -synuclein to bind the negatively charged vesicles (**Figure 3B-D**). The respective dissociation constants (K_d) (Supplementary Methods)⁴¹ were 5 μ M (95% confidence interval 3-10 μ M) and 6 μ M (95% confidence interval 3-20 μ M), respectively for non-acetylated and acetylated α -synuclein. The stoichiometry of α -synuclein and DMPS molecules was also calculated, where for acetylated α -synuclein the apparent number of lipid molecules per α -synuclein monomer was lower than for non-acetylated α -synuclein; with 17 DMPS molecules per acetylated monomer (95% confidence intervals of 10-23) and 29 DMPS molecules per non-acetylated monomer (95% confidence intervals of 22-35, **Figure S1**). The reduced stoichiometry for acetylated α -synuclein may explain the decreased α -helicity observed compared to the non-acetylated (**Figure 3C,D**).

The solubility of monomeric α -synuclein was then analysed under the conditions used for later kinetic assays (pH 4.8, 6.5 and 7.4) as a decreased solubility of proteins can impact their

aggregation propensity²⁸. Acetylated α -synuclein displayed similar behaviour to the non-acetylated α -synuclein in the presence of increasing concentrations of polyethylene glycol (PEG) across this pH range, indicating that the solubility of those two species is the same under the conditions that we analysed (**Figure 3E-G**).

The N-terminal acetylation of α -synuclein reduces the lipid-induced aggregation rate

We next investigated the effect of N-terminal acetylation on α -synuclein aggregation in the presence of lipid membranes. To this end, we used negatively charged DMPS vesicles, which were previously shown to induce α -synuclein aggregation⁴¹. Lipid-induced aggregation of α -synuclein is mediated by the binding of its positively charged N-terminus (**Figure 2**) to the negatively charged head groups of DMPS vesicles^{41,44}. Using ThT fluorescence intensity as a measure of fibril mass, we found that the rate of lipid-induced aggregation was decreased for acetylated α -synuclein with respect to non-acetylated α -synuclein (**Figure 4A-C**). The ThT fluorescence intensity at the end of the aggregation reaction, however, was increased for acetylated α -synuclein compared to non-acetylated α -synuclein (**Figure S2**), indicating either a higher level of monomer to fibril conversion or the formation of aggregate species with different ThT binding properties.

To further study the structure and morphology of the aggregates formed in the lipid-induced aggregation process, the lipid vesicles were removed by the addition of a detergent. The isolated aggregates were analysed by Fourier-transform infrared spectroscopy (FTIR) to determine the secondary structure, and by transmission electron microscopy (TEM) and atomic force microscopy (AFM) to determine their morphology (**Figure 4**). At 30 °C, the products of lipid-induced aggregation of non-acetylated α -synuclein are primarily kinetically-trapped protofibrils^{41,44,45}, which are characteristically thin (height < 5nm) and twisted, as we indeed observed by AFM for both acetylated and non-acetylated species (**Figure S2**). However, when the end products of the lipid-induced aggregation reaction of acetylated α -synuclein were analysed by TEM, mature fibrils were observed alongside the immature protofibrils, compared to only immature species for non-acetylated α -synuclein (**Figure 4C,D**). This result was further corroborated by the analysis of the FTIR spectra, which revealed a higher degree of β -sheet structure in the acetylated species (**Figure 4E,F**). The additional presence of mature fibrils at

the end of the acetylated α -synuclein aggregation reaction is likely the cause of the increased ThT fluorescence signal observed in the aggregation of acetylated α -synuclein (**Figure S2**).

The N-terminal acetylation of α -synuclein reduces fibril elongation and surface-catalysed fibril amplification

After the primary nucleation events to initiate α -synuclein aggregation, fibrils can act as catalysts to seed further aggregation. The seeding by α -synuclein fibrils has been associated with the cell-to-cell spreading of α -synuclein pathology, and previous studies have shown acetylated α -synuclein is more effective at seeding aggregation in cells⁴⁶. It has recently been shown that acetylated α -synuclein is recruited to fibrils by interactions involving the N-terminal 11 residues and intrinsically disordered regions of the fibril and oligomer surfaces⁴⁷. Therefore, we assessed how the N-terminal acetylation of α -synuclein impacted the secondary processes of aggregation by using conditions that favour fibril elongation or surface-catalysed fibril amplification, which includes both secondary nucleation and fibril elongation steps. By varying solution conditions, we can favour the aggregation processes in our reactions; by using a high concentration of seeds and pH 6.5, fibril elongation is favoured, but with a low concentration of seeds and an acidic pH we can favour secondary nucleation in the surface-catalysed fibril amplification reaction. Acidity in specific brain regions has been proposed to be important in the development of PD⁴⁸.

When compared with non-acetylated α -synuclein, acetylated α -synuclein showed reduced rates of both fibril elongation and fibril amplification in relation to non-acetylated α -synuclein (**Figure 5**). Non-acetylated α -synuclein fibrils have a higher seeding efficiency, suggesting that the small change in the N-terminus that forms part of the fuzzy coat of the fibril surface⁴⁹, may affect both the addition of monomers to fibril ends and the efficiency of surface-catalysed fibril amplification catalysed by fibril surfaces.

In 20 mM NaPO₄ pH 6.5 buffer, under shaking conditions, where it is likely all microscopic mechanisms occur⁵⁰, non-acetylated α -synuclein had a higher rate of aggregation compared to acetylated α -synuclein, and a higher ThT fluorescence plateau (**Figures 5D, S3 A**). A decreased ThT plateau signal for aggregated acetylated α -synuclein is consistent with previous studies⁵¹. However, in this bulk aggregation assay, where we used the same NaPO₄ buffer as in the lipid-induced aggregation, the structures of the resulting fibrils did not display significant differences

(**Figure S3C,D**), highlighting the significance of lipids in the aggregation of α -synuclein. When the bulk aggregation was carried out in PBS at pH 7.4, however, acetylated α -synuclein formed fibrils with different secondary structure (**Figure S3**), further highlighting the importance of solution conditions and aggregation processes in fibril structure and morphology.

The N-terminal acetylation of α -synuclein increases the formation of misfolded oligomers

Since α -synuclein oligomers are highly toxic species¹⁸, we investigated whether or not N-terminal acetylation affects the formation of oligomeric species in seeded aggregation and the structures of stabilised oligomers. The production of α -synuclein misfolded oligomers during the aggregation process was calculated using a model described recently (see Supplementary Methods), harnessing the observed rates of fibril elongation and secondary nucleation to predict the abundance of oligomers in the surface-catalysed fibril amplification reaction⁴⁰. We found that the N-terminal acetylation of α -synuclein increases the flux towards misfolded oligomeric species. Although the onset of oligomer production was delayed with an increased lag time, the height of the predicted oligomer peaks was higher in acetylated α -synuclein, indicating a larger concentration of oligomer species over time (**Figure 6**). As we calculated a difference in oligomer flux, our results indicate that the rate of surface-catalysed fibril amplification (which includes both secondary nucleation at the fibril surface and fibril elongation at fibril ends) is reduced for acetylated α -synuclein.

In addition to probing the concentrations of oligomers produced during the aggregation process, we also compared the structures of kinetically trapped oligomers of non-acetylated and acetylated α -synuclein, which were produced by a well-established protocol⁵². Analysis by FTIR indicated no structural differences between these two species, as both displayed similar degrees of β -sheet content, a parameter which has previously been linked with oligomer toxicity, in keeping with previous results¹⁸ (**Figure S4**).

N-terminal acetylation alters the morphology and secondary structure, but not the stability, of α -synuclein fibrils

In order to obtain more insights into the links between the effects of N-terminal acetylation of α -synuclein on the thermodynamics, kinetics and cytotoxicity of α -synuclein aggregates, we studied the effects of this post-translational modification on the stability, morphology and structure of the fibrils.

We first probed the morphology of the fibrils, as this could also impact their seeding capacity. Although TEM images of fibrils from both α -synuclein variants showed similar fibrils (**Figure 7A,B**), we found that pre-formed fibrils (PFFs, see Methods) from non-acetylated α -synuclein were significantly shorter than those formed by acetylated α -synuclein (**Figure 7C**). Using CD and FTIR, we then compared the secondary structure of the fibrils formed by non-acetylated and acetylated α -synuclein (**Figure 7D,F**). By CD, both non-acetylated and acetylated α -synuclein fibrils appeared to have primarily β -sheet secondary structure, with a characteristic single minimum around 220 nm. However, the spectrum for acetylated α -synuclein fibrils was broader, suggesting the presence of additional secondary structure elements. These results were consistent with those obtained by FTIR, with both α -synuclein fibrils secondary structure being dominated by β -sheet with a peak 1624 cm^{-1} , but with acetylated α -synuclein fibrils having a significantly increased level of other secondary structures (α -helix or disordered) indicated by the presence of a peak at 1654 cm^{-1} . FTIR deconvolution showed that acetylated α -synuclein fibrils have significantly ($p < 0.01$) more disordered and α -helical content compared to non-acetylated α -synuclein fibrils. Furthermore, acetylated α -synuclein fibrils had significantly ($p < 0.01$) less β -sheet content than was observed in non-acetylated α -synuclein fibrils (**Figure 7E**). In good agreement with the structural differences we observed by CD and FTIR spectroscopies, partial digestion with proteinase K (PK) indicated an increase in PK accessibility for the AcWT fibrils as compared to the WT fibrils (**Figure 7G**). This is in good agreement with the proteinase K digestion pattern previously reported for fibrils formed under slightly different aggregation conditions⁵¹ and confirms that our AcWT fibrils contain more disordered regions. In the former study, they also found that AcWT fibrils have different morphological properties compared to WT fibrils; however, they reported that the amyloid core structure of AcWT fibrils were similar to the non-acetylated fibrils⁵¹. For non-acetylated α -synuclein fibrils multiple polymorphic structures have been observed, differing in protofibril interface residues, helical rise and twist and the number of residues with defined secondary

structure in the fibril core⁵³. There is a structure for N-terminally acetylated α -synuclein fibrils that resembles one of these non-acetylated α -synuclein fibril polymorphs⁵⁴, however it is also likely that acetylated α -synuclein fibrils can take multiple structural forms. It would be highly relevant to characterise the structures of these species using high-resolution techniques such as cryo-EM.

The stability of the fibrils was assessed by their response to the denaturant guanidine hydrochloride (GdnHCl) (**Figure 7H**). The sensitivity of fibrils towards GdnHCl-induced denaturation did not vary significantly between non-acetylated and acetylated α -synuclein fibrils. Both fibrillar species appeared to be highly dynamic and showed dissociation at low concentrations of denaturant, suggesting that under destabilising conditions α -synuclein fibrils may release monomeric and oligomeric forms through a mechanism independent of surface-catalysed fibril amplification.

The N-terminal acetylation does not modify the cytotoxicity of α -synuclein fibrils and fibril fragments

Aggregates of α -synuclein are toxic to cells and induce cell stress and death^{55,56,57}. Furthermore, previous studies have shown that acetylated α -synuclein is taken up by neuronal cells in a manner distinct to non-acetylated α -synuclein⁴⁶. Since we observed different morphologies and secondary structure for acetylated and non-acetylated α -synuclein aggregates (**Figure 7**), we assessed how N-terminal acetylation of α -synuclein affects the cytotoxicity of its aggregates. As fragmented fibrils have an increased toxicity compared to full length mature fibrils⁵⁸, we used the sonicated pre-formed fibrils (PFFs) to induce cellular cytotoxicity. PFFs have been used to induce toxicity in mice models by injecting short fibrils of α -synuclein directly into the striatum and shown to recapitulate the phenotypes and spreading of PD, including loss of dopaminergic neurons and reduction of striatal dopamine terminals and motor behaviour defects^{57,58}.

To investigate the cytotoxicity of non-acetylated and acetylated α -synuclein PFFs, we took a two-pronged approach to measure both the impact on live and dying cells with Calcein AM and propidium iodide (PI). Calcein AM is a dye that permeates live cells and is converted to fluorescent calcein by intracellular esterases and therefore acts as a live cell dye for viability measurements⁵⁹. PI penetrates dead and dying cell membranes, once inside cells PI intercalates with DNA to become fluorescent; however, it cannot penetrate live cells and can therefore be

used as a cell viability marker^{60,61}. Our results using non-differentiated SH-SY5Y cells indicate no significant difference in the cytotoxicity of the PFFs derived from either non-acetylated or acetylated α -synuclein, as assessed by Calcein AM and PI fluorescence (**Figure 8**). We also tested the effects of stabilised oligomers from both acetylated and non-acetylated α -synuclein on the viability of SH-SY5Y cells (**Figure S4 C**). Consistent with previous studies¹⁸, we found there was no significant difference in the toxicity induced by the two species.

When comparing the impact of non-acetylated and acetylated α -synuclein PFFs we also found the two variants induced comparable levels of reactive oxygen species (ROS) as measured by dihydrorhodamine (DHR) fluorescence, and disruption of mitochondrial membrane potential, measured by MitoTracker Deep Red (MTDR) fluorescence (**Figure 9**). Previous studies have found little difference in the cellular localisation and distribution of non-acetylated and acetylated α -synuclein⁶², this may explain the similarity in toxicity we observed for the two species.

Conclusions

The results that we have reported in this work show that N-terminal acetylation retards the aggregation of α -synuclein and alters the secondary structure, length and morphology of α -synuclein fibrils. We have found in particular that this post-translational modification slows down the aggregation of α -synuclein in the presence of lipid vesicles, while leading to more structured aggregates. Our results also indicate that the N-terminal acetylation increases the reactive flux towards the overall amount of transient misfolded oligomers during the α -synuclein secondary nucleation process. Given that different oligomeric species may give rise to different levels of neurotoxicity^{63,64} it will be important to investigate further the effects of N-terminal acetylation on the lipid-dependent aggregation of α -synuclein for lipid membranes of compositions corresponding to those of synaptic vesicles, endosomes, mitochondria and other cell membranes.

Materials and Methods

Protein production. α -Synuclein (UniProt accession code P37840) was produced by transforming *E. coli* with an expression pT7-7 plasmid. N-terminal acetylated α -synuclein was produced by co-transforming *E. coli* with the same plasmid and an expression pACYCduet plasmid encoding a yeast N-terminal acetyltransferase (NatB), provided by Dr. Dan Mulvihill, University of Kent, Canterbury, UK (Johnson *et al.*, 2010). Acetylated α -synuclein and non-acetylated α -synuclein were then purified in 20 mM NaPO₄ pH 6.5 buffer, as described previously⁶⁵. The presence of N-terminal acetylation was verified by mass spectrometry, and the protein concentrations were determined by absorbance at 275 nm using the extinction coefficient α -synuclein $\epsilon = 5600 \text{ M}^{-1}\text{cm}^{-1}$ ⁶⁶. Aliquots were flash frozen in liquid N₂ and stored at -80 °C.

Binding to lipid membranes. DMPS small unilamellar vesicles (SUVs) were prepared as described previously⁴¹, by cycles of freeze/thaw followed by sonication. DMPS vesicles were added to monomeric α -synuclein and the binding event was measured by CD spectroscopy. CD spectra were obtained on a JASCO J-810 (Easton, USA) using quartz cuvettes with path lengths of 1 mm, by averaging 15 individual spectra recorded between 250 nm and 200 nm, with a bandwidth of 1 nm, a data pitch of 0.2-0.5 nm, a scanning speed of 50 nm/min and a response time of 1 s. The relative compositions of secondary structure were obtained using an online server Bestsel⁶⁷. To analyse the binding affinity of both acetylated α -synuclein and non-acetylated α -synuclein, the data were fitted using a previous model⁴¹.

FTIR spectroscopy. FTIR spectra were recorded on a Bruker Vertex 70 FTIR (Billerica, USA) on the diamond ATR, with 4 cm resolution and a data range of 800 – 4000 cm⁻¹ wavelengths; the data in the amide peak 1 (1580 – 1720 cm⁻¹) were analysed. A rubber band baseline correction was applied to the data, before fitting to a Gaussian equation with 4 – 7 peaks. The area under each peak was integrated to obtain relative compositions of secondary structure using the following classifications: peaks under 1640 cm⁻¹ were assigned to β -sheets structures, peaks from 1640 to 1660 cm⁻¹ were assigned to disordered random coils / α -helices, and peaks above 1660 and 1685 cm⁻¹ were also assigned to β -sheet structures.

Solubility assay. Solubility was measured using a PEG-precipitation assay. In this assay one measures protein precipitation for increasing concentrations of PEG. The midpoint value (PEG_{1/2}) is correlated with the solubility. Monomeric α -synuclein was incubated with increasing concentrations (0-30%) of PEG-6000 at 4 °C for 2 days in 384-well plates. The plates were centrifuged to pellet aggregates and the supernatant was transferred into a fresh 384-well plate. The monomeric α -synuclein concentration in the supernatant was measured by absorbance. This assay was conducted using the same buffer (20 mM NaPO₄ pH and respective pH) specified below for the aggregation reactions and at pH 7.4 also.

Aggregation kinetics. To assess the microscopic steps of α -synuclein aggregation, experiments were carried out using different conditions favouring different processes (lipid vesicle induced aggregation, fibril elongation and surface-catalysed fibril amplification), all with a range of α -synuclein concentrations from 20 - 100 μ M, and 50 μ M ThT^{39,41,44} (**Table 1**). For the lipid-induced aggregation assay, the concentration of DMPS used was chosen based on previous studies to maintain a low ratio of DMPS/ α -synuclein, to allow both free α -synuclein and lipid vesicle states to be present, keeping the aggregation rate high⁴¹. All assays were set up in triplicate in 96 half-well plates (Corning 3881, non-binding, clear bottomed, Corning, Tewksbury, USA) sealed with aluminium foil and ThT fluorescence was detected in quiescent conditions on FLUOstar plate readers (BMG Labtech, Aylesbury, UK), with excitation and emission wavelengths of 440 and 480 nm, respectively.

Aggregation assay	Buffer conditions	Temperature
Lipid-induced aggregation	20 mM NaPO ₄ , pH 6.5, 100 μ M DMPS	30 °C
Surface-catalysed fibril amplification	20 mM NaPO ₄ , pH 4.8, 50 nM seed	37 °C
Fibril elongation	20 mM NaPO ₄ , pH 6.5, 2.5 - 5 μ M seed	37 °C

Aggregation kinetics under shaking conditions. To complement the three-pronged strategy described above and observe the effects of N-terminal acetylation on α -synuclein aggregation in bulk, a shaking method was used in 20 mM NaPO₄ pH 6.5. α -Synuclein monomers (70 μ M)

were incubated in Corning 3881 plates in triplicate, 37 °C, with 50 µM ThT and addition of a single glass bead (3 mm diameter) to each well. Aggregation was stimulated by shaking at 200 rpm.

Fibril preparation. First generation (F0) fibrils of N-terminal acetylated α -synuclein and non-acetylated α -synuclein were produced by concentrating the monomeric protein to > 600 µM and then by incubating for 72-96 h at 40 °C, with 1,500 rpm stirring with a Teflon stirrer bar. Fibrils were then sonicated (low power, 50% pulse, 15 s) and left to incubate for a further 24-48 h. The resulting fibrils were pelleted by centrifugation at 15,000 rpm and any remaining monomer removed. Second generation (F1) fibrils were prepared by seeding with 10% concentration of fresh F0 fibrils to monomeric protein concentration. After seeding, the F1 fibrils were sonicated and incubated in the same way as described above. Remaining monomer was again removed by centrifugation, and fibrils were used immediately. Fibril concentrations were measured by dissociating the fibrils in a total solution of 4 M GdnHCl and then measuring the absorbance at 275 nm with the extinction coefficient α -synuclein $\epsilon = 5600 \text{ M}^{-1}\text{cm}^{-1}$ ⁴¹.

Protofibril isolation. In order to characterise the end point species of lipid induced aggregation, aggregates were isolated from the lipid vesicles. N-Lauryl sarcosine sodium salt was added at a 1:1 w/v ratio and samples were incubated at 37 °C, 1 h. The aggregates were pelleted and washed, by ultracentrifugation (120,000 rpm, 1 h, 20 °C) and resuspended in 20 mM NaPO₄ pH 6.5 three times. The concentration of monomer in the aggregates was measured as described above for fibrils.

Preparation of stabilised misfolded oligomers. Stabilised misfolded oligomers were prepared following a previously described method ⁵². Briefly, monomeric α -synuclein at a concentration of ~ 850 µM was dialysed into water, lyophilised, resuspended in PBS and then incubated at 37 °C for 20 – 24 h. Large aggregated species were removed by ultracentrifugation (1 h, 288,000 x g), and excess monomeric or small oligomeric species were removed by 100 kDa cut off centrifugation filters. The concentration of monomer in the oligomer samples was measured by absorbance at 275 nm as described for fibril species.

Proteinase K digestion of fibrils. Aliquots of the fibril reactions (50 µl) were centrifuged (5 min, 20,000 rcf, RT). The supernatant was removed, and the fibrils were resuspended in 50 µl

PBS. To this, proteinase K (0.05 mg/ml final concentration) was added, and the samples were incubated (37°C, 45 min). The reactions were centrifuged, and the supernatant was removed, 7M Urea (25 µl) and 4X LDS loading buffer (5 µl) was added and heated at 95°C for 5 min. Monomeric α -synuclein (25 µM) was also treated with proteinase K (0.05 mg/ml final concentration) and incubated (37°C, 45 min) for comparison. Samples were run on a 15% SDS-PAGE gel and stained with Coomassie blue.

Fibril stability. To determine the stability of α -synuclein fibrils, a depolymerisation assay approach was applied. Fibrils were incubated overnight at 25 °C at increasing concentrations of GdnHCl (0 - 4 M). Then, samples were centrifuged (15 min, 21130 x g, 20 °C), and the supernatant collected. The concentration of monomeric α -synuclein that had dissociated from fibrils was estimated using a Pierce BCA Protein Assay Kit (ThermoFisher).

Fibril morphology. Fibril morphology was analysed by transmission electron microscopy (TEM) and atomic force microscopy (AFM). For the TEM analysis, fibrils were diluted to 5-10 µM and incubated on carbon coated copper grids for 3-4 min before washing with distilled water (dH₂O) and staining with uranyl acetate (2 % w/v) for 2 min and then washed again with dH₂O. TEM images were taken on a Tecnai G2 80-200kv transmission electron microscope (ThermoScientific, at the Cambridge Advanced Imaging Centre (CAIC), University of Cambridge), with magnifications of 9-14k. ImageJ was used for length analysis. The same protocol was applied to protofibrils, they were imaged on a Talos F200X G2 TEM (ThermoScientific, Department of Chemistry, University of Cambridge).

AFM samples were prepared following a method previously described⁴⁴. Fibrils were diluted to 1 µM in dH₂O, 50 µl was deposited onto freshly cleaved mica and incubated for 45 min before washing with 50 µl dH₂O. All samples were imaged on a NX10 Atomic Force Microscope (Park Systems, Suwon, South Korea), using non-contact mode. Areas of 4 µm x 4 µm were imaged in 1024 pixels at a speed of 0.3 – 0.4 Hz. Images were analysed by SPIP software (Image Metrology, Hørsholm, Denmark), to determine the height and length of aggregates.

Cell culture. We used genetically confirmed, mycoplasma-free human SH-SY5Y neuroblastoma cells (A.T.C.C., Manassas, USA). The cells were cultured in Dulbecco's Modified Eagle Medium F-12 Nutrient Mixture + GlutaMaxTM (Gibco, Waltham, USA) with 10% v/v fetal bovine serum (Gibco, Waltham, USA) referred to as SH media. The cells were

grown in T-75 cell culture flasks (CELLSTAR, Stonehouse, UK) in a 5.0% CO₂ humidified atmosphere at 37 °C. Cells were passaged when they were 70-80% confluent.

Cell viability assays. SH-SY5Y cells were plated at a concentration of 10,000 cells per well in a 96-well plate with lid (3603, Corning) in SH media at a total volume of 200 µl. Surrounding wells were filled with 100 µl sterile PBS to ensure a homogeneous temperature across the plate. The cells were incubated at 37 °C for 24 h. The next day, the medium was removed and 200 µl of fresh SH medium with or without treatments was added (0.3, 0.03, or 0.003 µM of the PFFs, PBS, or 0.01% Triton X-100, all treatments were diluted so that they were diluted 10 times in appropriate volume of SH media). Each treatment was assessed in sextuplets in a single experiment, and each experiment was repeated at least three times.

For the Calcein AM assay, the SH media was removed from all wells, and cells were washed twice with PBS before a solution of 3 µM Calcein AM in PBS added and incubated for 30 min at 37 °C. Calcein AM fluorescence was then measured at 485nm/535nm excitation/emission. For PI fluorescence assays the SH media was removed from all wells, a solution of 2.5 µM PI in PBS was then immediately added and incubated for 30 min at 37 °C. PI fluorescence was then measured at 530nm/620nm excitation/emission. The background level of PI fluorescence was then calculated by removal of PI in PBS solution from all wells, fresh PBS was then added to wells before a second fluorescence measurement taken at 530nm/620nm. Significant differences in results were identified by one-way ANOVA analysis.

Cell toxicity. Flow cytometry experiments were completed following a previously described protocol⁶⁸. Briefly, cells were resuspended in PBS with no treatments (unstained control), or with 0.1 mM dihydrorhodamine 123 (DHR), and 100 nM MitoTracker Deep Red (MTDR), following no treatment, or treatment with ROS inducing controls 10 µM carbonyl cyanide 3-chlorophenylhydrazone (CCCP), or 10 µM menadione, or with PFFs from non-acetylated or acetylated α -synuclein at 0.3 – 0.03 µM. CCCP is a proton ionophore that induces oxidative by dissipating mitochondrial membrane proton gradient⁶⁹ and menadione also induces oxidative stress in the mitochondria and cytosol, and decreases the mitochondrial membrane potential⁷⁰. Cells were incubated for 30 min at 37 °C, then pelleted by centrifugation (250 x g, 5 min), and resuspend in PBS and held on ice until analysed by flow cytometry; 10,000 events were acquired for all samples. Samples were run on a Cytoflex (Beckman), with excitation/emission at 488 nm and 525/40 nm respectively for DHR and excitation/emission at 638 nm and

660/10nm for MTDR. DHR is lipophilic and can pass through cell membranes. In cells DHR is oxidised by free the reactive oxygen species (ROS), H₂O₂ or peroxynitrite, to a fluorescent product ⁷¹. MTDR is also lipophilic and can permeate cell membranes, where it associates with mitochondria. MTDR is mitochondrial membrane potential sensitive, depolarisation decreases fluorescence whilst increased potential increases fluorescence ⁷². Significant differences in results were identified by one-way ANOVA analysis.

Accession codes

α -synuclein: UniProt P37840

Acknowledgements

The authors thank Dr Daniel Mulvihill for the plasmid to express the *N*-acetylation B complex, the Cambridge Advanced Imaging Centre and the TEM facility and Dr Heather Greer (EPSRC grant EP/P030467/1) for the use of their equipment. J.R.K. is supported by an MRC Career Development Award (MR/W01632X/1).

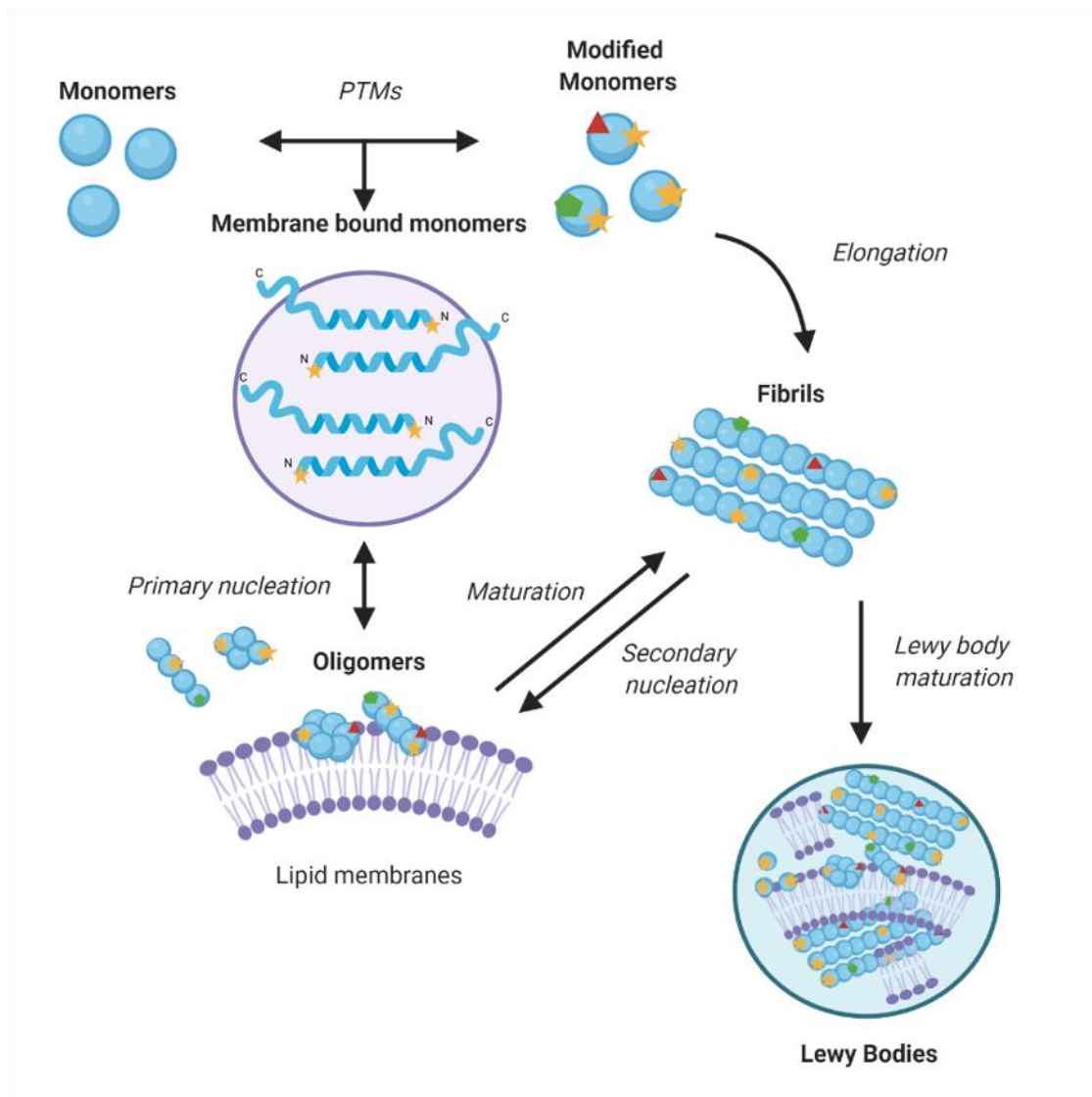


Figure 1. A model of α -synuclein aggregation. As α -synuclein does not readily aggregate spontaneously, it has been proposed that lipid membranes are the site of the primary nucleation events that initiate the process of α -synuclein aggregation *in vivo* ⁷³. At first, monomers nucleate to form small disordered oligomeric species, which then either dissociate and return to the monomeric pool or grow into amyloid aggregates ^{17,74}. The process of Lewy body formation may involve such aggregates and lipid membranes ^{75,6}.

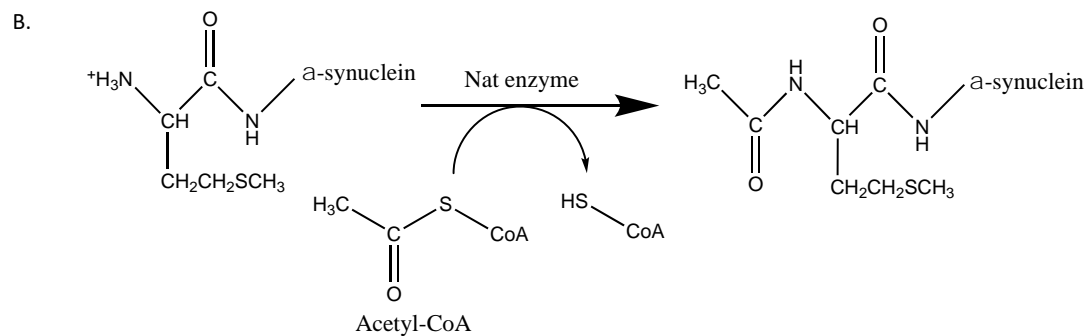
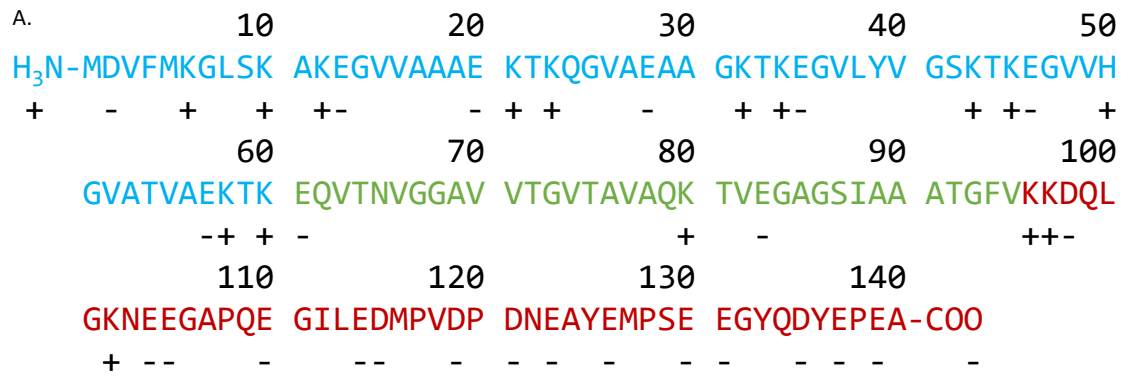


Figure 2. Amino acid sequence of α -synuclein and N-terminal acetylation. (A) Primary sequence of α -synuclein. The N-terminal region (residues 1-60) is shown in blue, the non-amyloid- β component (NAC, residues 61-95) in green, and the negatively charged unstructured C-terminal domain (residues 96-140) in red; positively charged residues are indicated by a + and negatively charged ones by a -. (B) N-terminal acetylation of the -1 Met of α -synuclein. This post-translational modification is carried out by a N-terminal acetyltransferase enzyme. N-terminal acetylation leads to the loss of a positive charge at the N-terminus of α -synuclein.

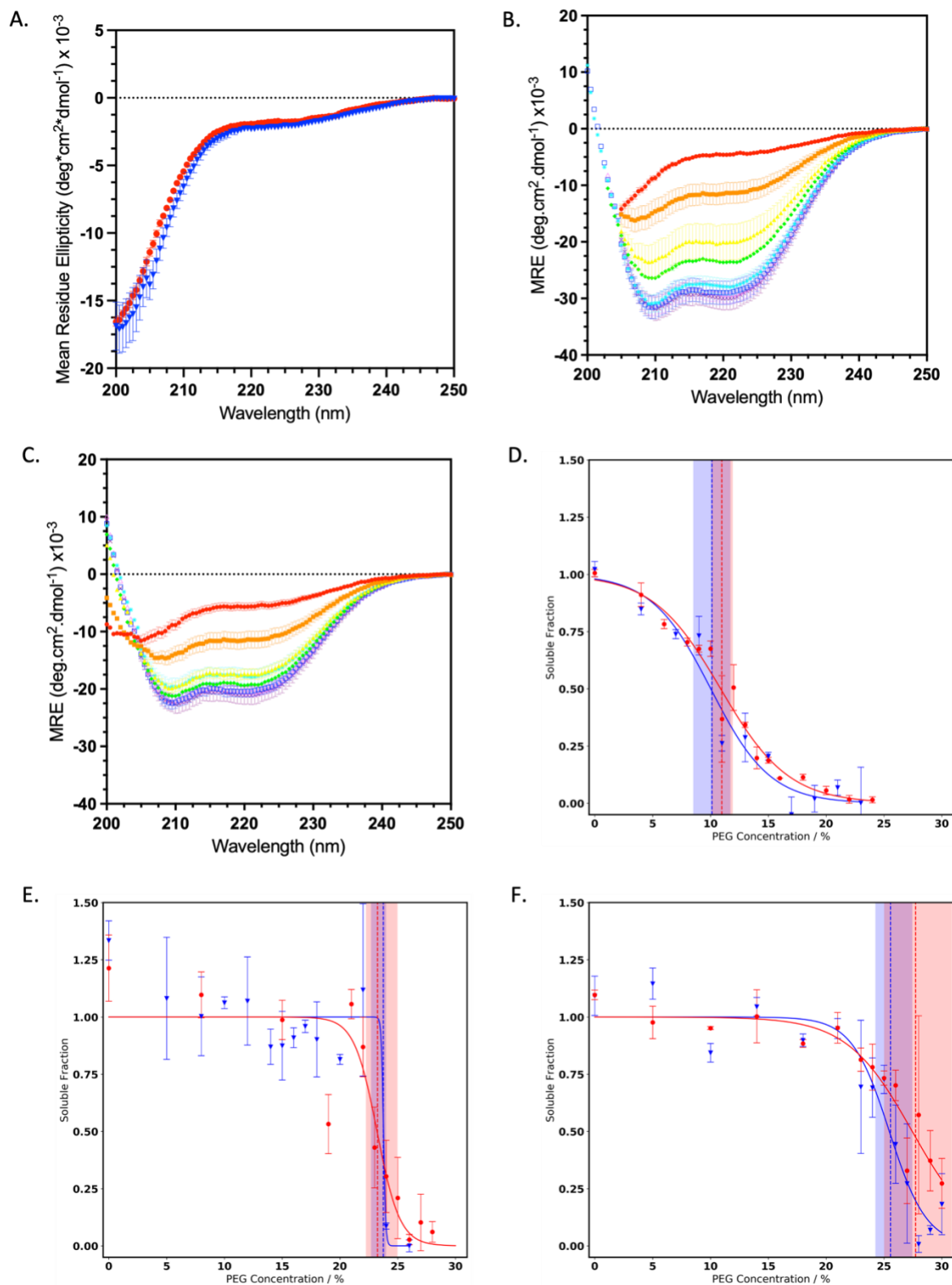


Figure 3. The structural properties and the solubility of monomeric α -synuclein are only slightly affected by N-terminal acetylation. (A) Far UV CD spectra of non-acetylated α -synuclein (blue triangle) and N-terminal acetylated α -synuclein (red dot) monomers; error bars

represent the standard error of the mean (SEM) with $n = 3$ (**B,C**) CD spectra of non-acetylated α -synuclein (**B**) and acetylated α -synuclein (**C**), in the presence of increasing concentrations of DMPS: 0.1 mM (red), 0.25 mM (orange), 0.5 mM (yellow), 0.75 mM (green), 1 mM (cyan), 1.5 mM (blue), 2 mM (lilac) and 3 mM (purple); mean residue ellipticity (MRE), and error bars represent the SEM with $n = 3$. (**D-F**) The solubility of monomeric α -synuclein was measured by incubation with increasing concentrations of PEG at pH 4.8 (**D**), pH 6.5 (**E**) and pH 7 (**F**) for non-acetylated α -synuclein (blue) and acetylated α -synuclein (red). The dashed lines represents the PEG_{1/2} value (which is correlated with the solubility) with confidence intervals represented by shaded areas; error bars indicate the standard error of the mean (SEM).

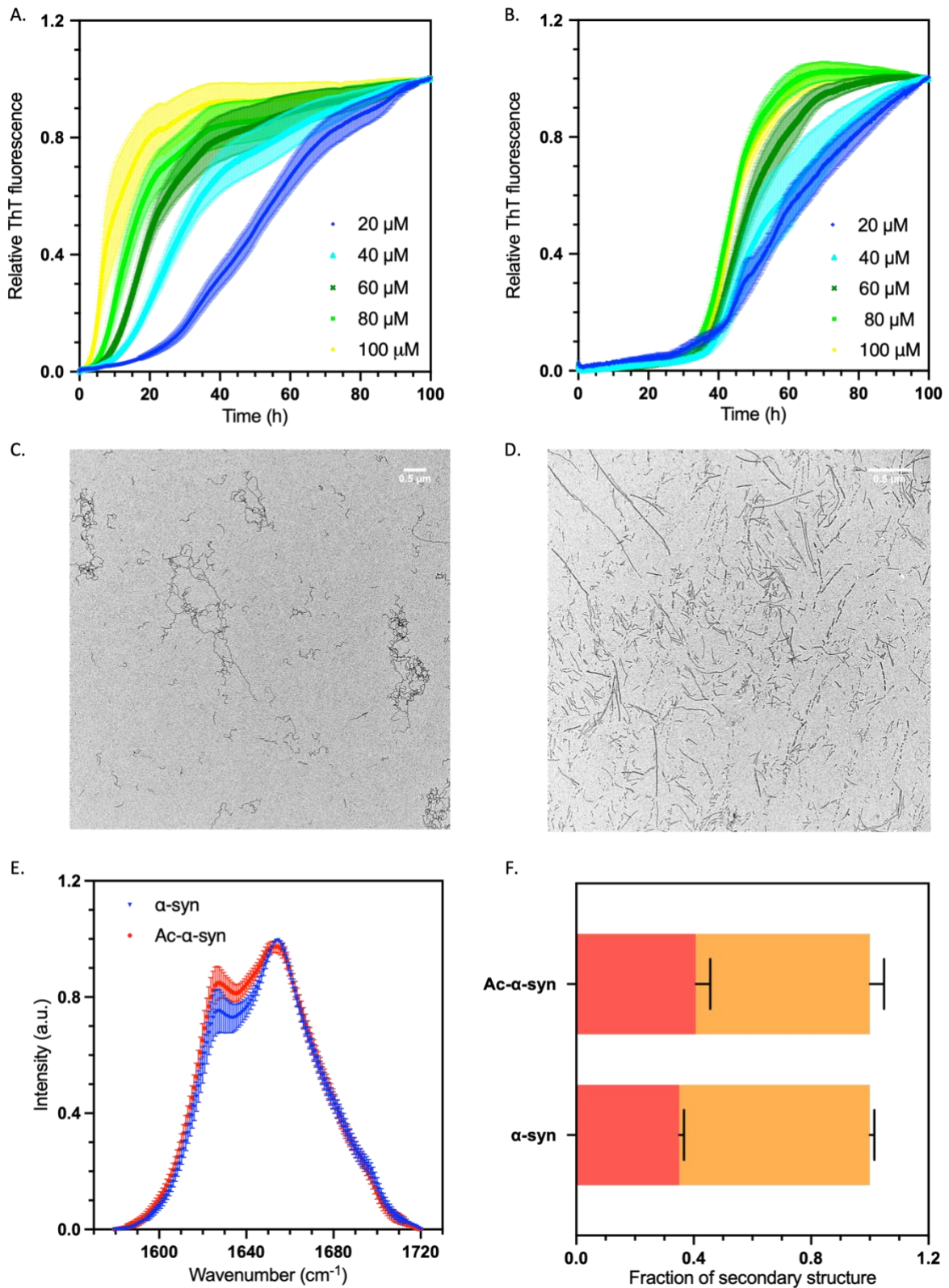


Figure 4. N-terminal acetylation delays the lipid-induced aggregation of α -synuclein. (A,B) Representative time course of a lipid-induced aggregation assay of non-acetylated (A) and acetylated α -synuclein (B); error bars represent the SEM of three repeats. Data were

normalised to the end point ThT fluorescence values for each reaction. Increasing initial concentrations of α -synuclein monomers added to the reaction are shown: 20 μ M (dark blue), 40 μ M (light blue), 60 μ M (dark green), 80 μ M (light green), and 100 μ M (yellow). Aggregation conditions were as follows: 20 mM NaPO₄ buffer, pH 6.5, 100 μ M DMPS; error bars represent the SEM with n = 3. **(C, D)** TEM images at 6.5k magnification of the end point of the aggregation reaction from panels A and B respectively; the scale bar represents 500 nm. **(E) Normalised** FTIR spectra of isolated aggregation end products of non-acetylated (blue triangles) and acetylated α -synuclein (red circles); error bars represent the SEM with n = 3. **(F)** Deconvolution of the FTIR spectra into secondary structural content for non-acetylated and acetylated α -synuclein, β -sheet shown in red and α -helix/disordered shown in orange; error bars represent SEM of n = 3.

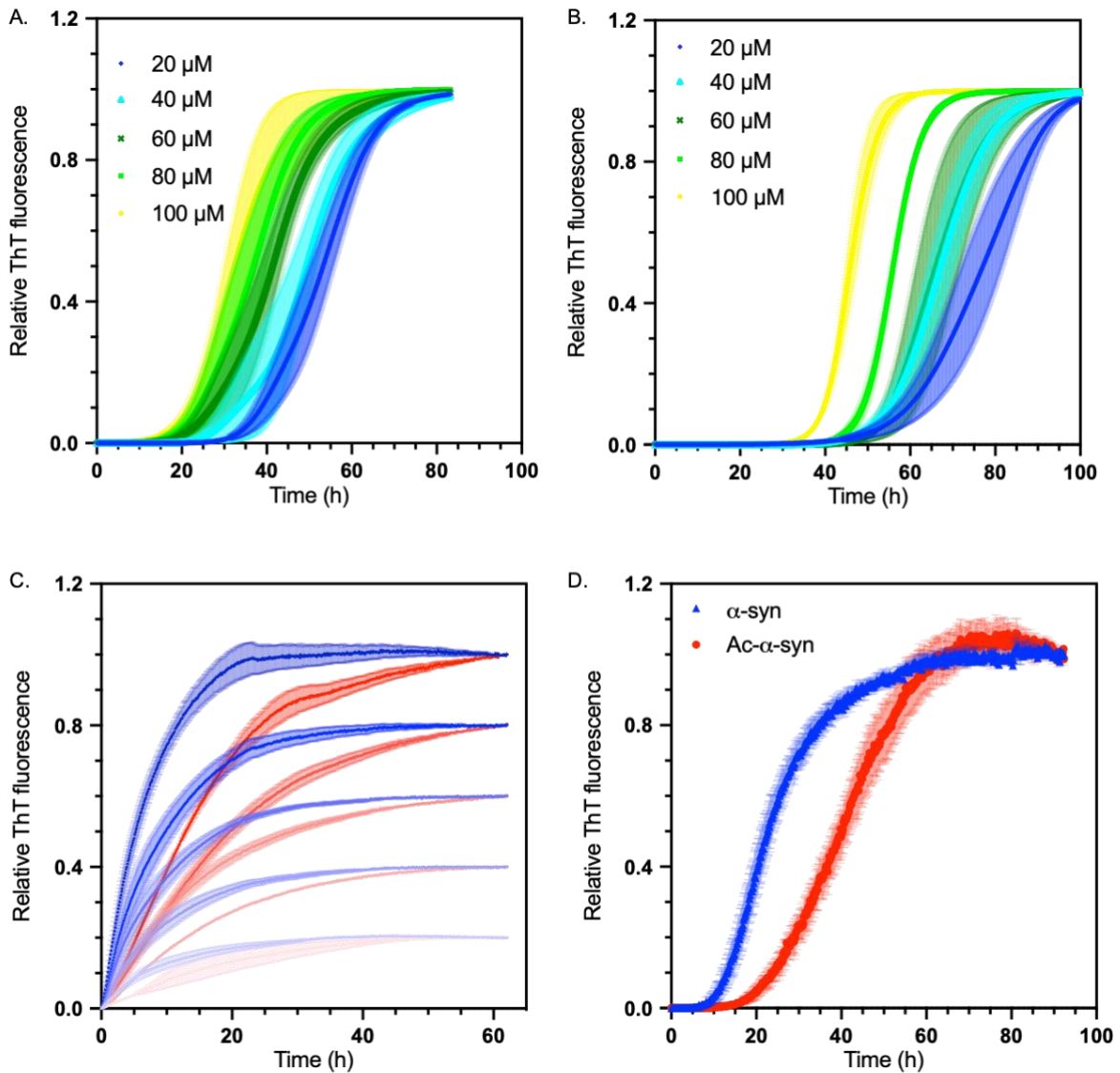


Figure 5. N-terminal acetylation delays secondary processes and fibril elongation of α -synuclein (A) Representative time courses of surface-catalysed fibril amplification of non-acetylated α -synuclein monomer seeded by non-acetylated α -synuclein fibrils. (B) Representative time courses of surface-catalysed fibril amplification of acetylated α -synuclein monomer seeded by acetylated α -synuclein fibrils. (A, B) Data were normalised to the end point ThT fluorescence values for each reaction. Increasing initial concentrations of α -synuclein monomers added to the reaction are shown: 20 μ M (dark blue), 40 μ M (light blue), 60 μ M (dark green), 80 μ M (light green), and 100 μ M (yellow). Aggregation conditions were as follows: 20 mM NaPO₄ buffer, pH 4.8, 50 nM seeds, under quiescent conditions; error bars represent the SEM, over three replicates. (C) Representative time courses of fibril elongation of non-acetylated α -synuclein monomer seeded with non-acetylated α -synuclein fibril (blue), acetylated α -synuclein monomer seeded with acetylated α -synuclein fibril (red).

Increasing concentrations are represented by increasing colour with 20 μM represented as the lightest, 40 μM , 60 μM , 80 μM and 100 μM as the darkest. Aggregation conditions were as follows: 20 mM NaPO_4 buffer, pH 6.5, 2.5 μM seeds, under quiescent conditions at 37 °C. **(D)** Analysis of aggregation in an unseeded shaking reaction, of non-acetylated α -synuclein (blue triangle) and acetylated α -synuclein (red dot); error bars represent the SEM with $n = 3$.

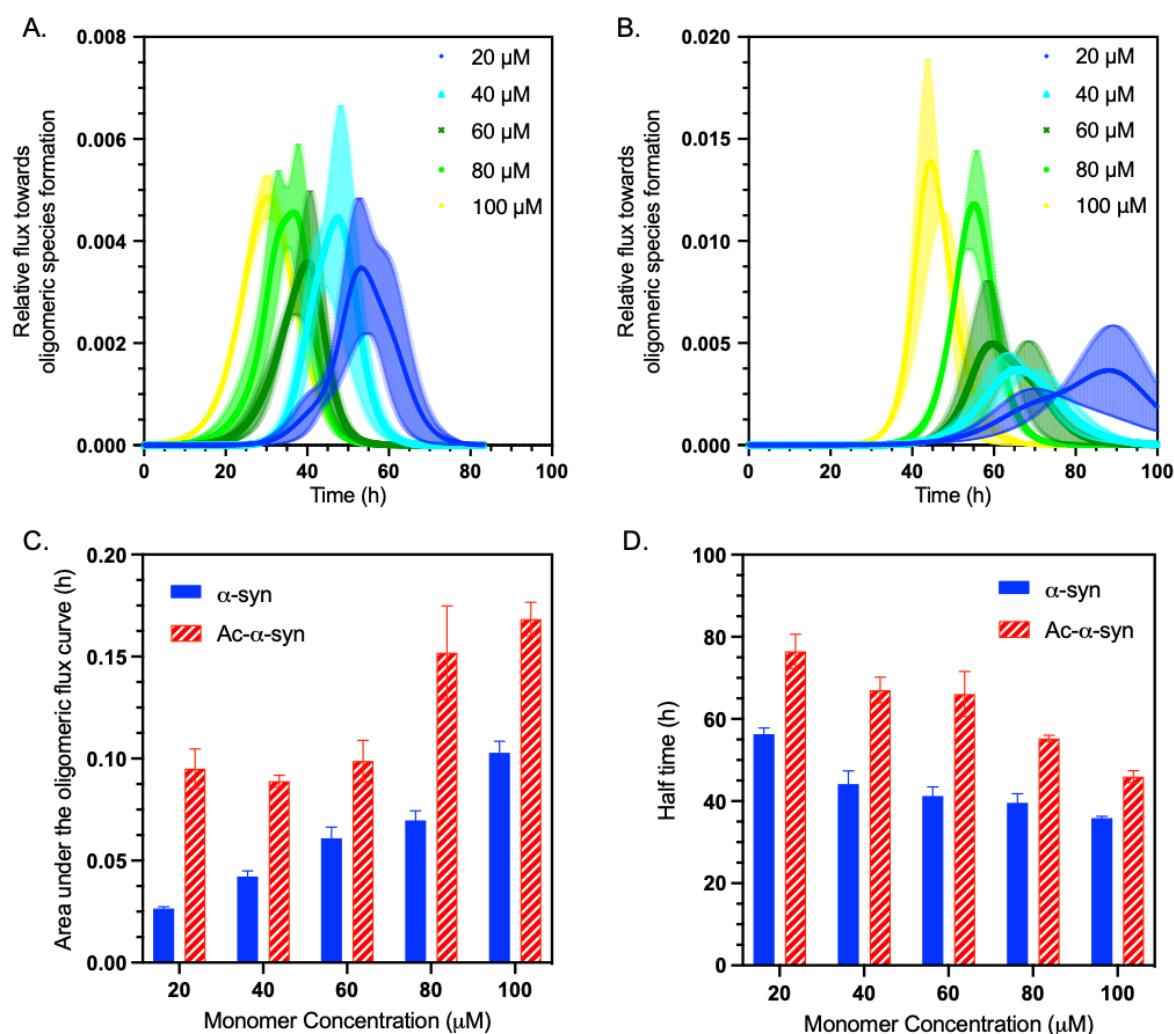


Figure 6. The N-terminal acetylation of α -synuclein increases the oligomer populations generated during aggregation. (A,B) Relative flux towards oligomeric species formation (Φ) of non-acetylated (A) and acetylated α -synuclein (B) generated from surface-catalysed fibril amplification data in **Figure 5**; error bars represent the SEM with n = 3. (C) Area under the curve (Φ AUC) for non-acetylated (blue) and acetylated α -synuclein (red) as a function of monomer concentration; error bars represent the SEM with n = 3. (D) Half time of the surface-catalysed fibril amplification reactions for non-acetylated (blue) and acetylated α -synuclein (red) as a function of monomer concentration error bars represent the SEM with n = 3.

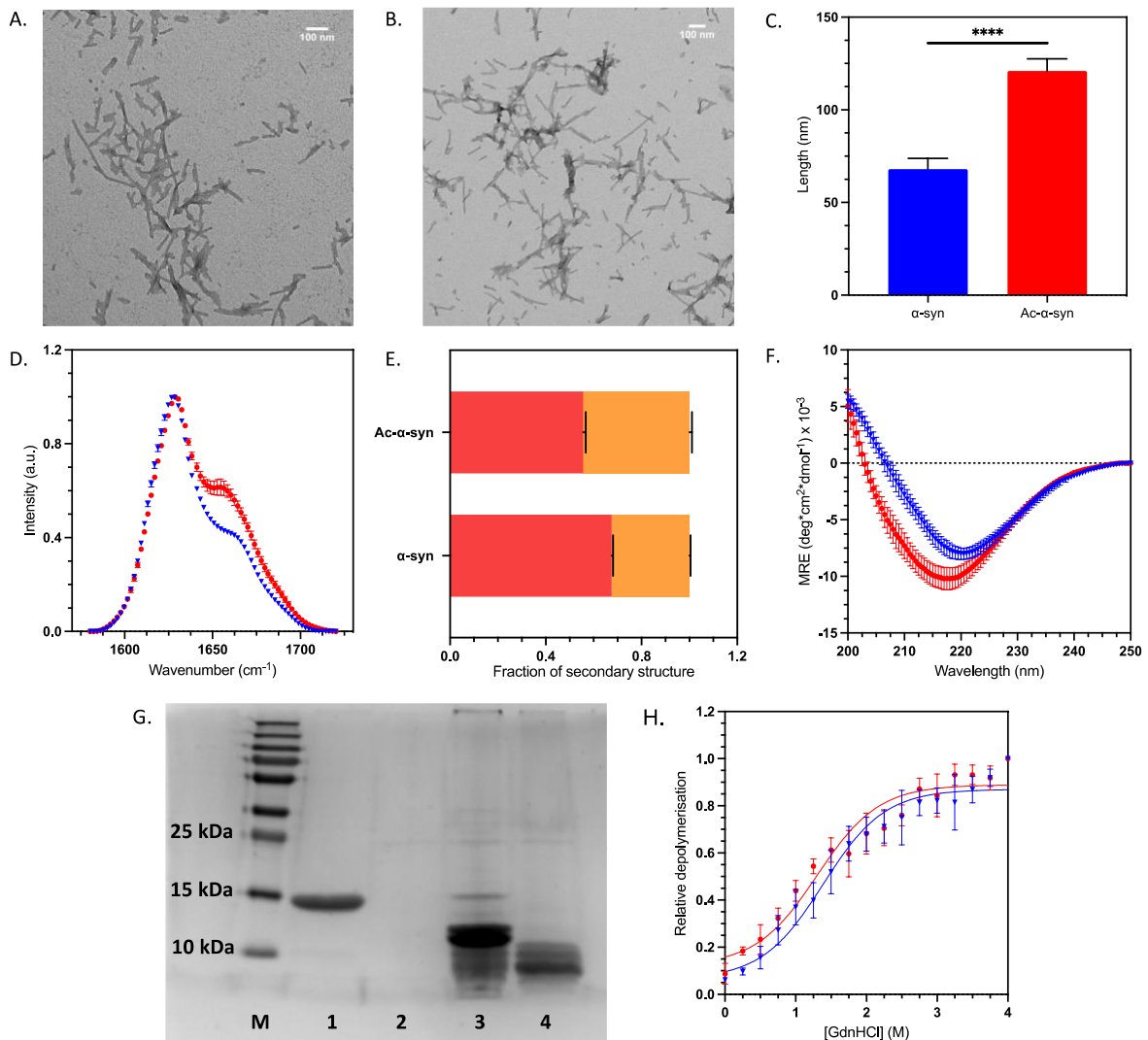


Figure 7. N-terminal acetylation alters the morphology and secondary structure, but not the stability, of α -synuclein fibrils. (A,B) TEM images of F1 α -synuclein fibrils, at 14.5k magnification non-acetylated (A) and acetylated α -synuclein (B) with scale bars of 100 nm (upper right corners). (C) Average length of pre-formed fibrils (PFFs) calculated by TEM image analysis. The statistical significance was assessed by an unpaired T-test. (D) Normalised FTIR F1 fibrils: non-acetylated α -synuclein (blue triangle) and acetylated α -synuclein (red dot); error bars represent SEM of $n = 3$. (E) Deconvolution of the FTIR spectra into secondary structural elements. β -sheet shown in red and α -helix/disordered shown in orange (F) Far UV CD spectra of F1 fibrils: non-acetylated α -synuclein (blue triangle) and acetylated α -synuclein (red dot), Error bars represent SEM of $n = 3$, MRE = mean residue ellipticity. (G) SDS-PAGE gel of proteinase K (PK) digests. Lanes are as follows: (M) PageRuler plus protein ladder, (1) non-acetylated α -synuclein monomer, (2) α -synuclein monomer + 0.05 mg/ml PK, (3) non-acetylated α -synuclein fibrils + 0.05 mg/ml PK, (4) acetylated α -synuclein fibrils + 0.05 mg/ml PK (H) Depolymerisation curve using GdnHCl as

a denaturant, the concentration of the soluble fraction was measured to observe fibril depolymerisation of non-acetylated α -synuclein (blue triangle) and acetylated α -synuclein (red dot), Error bars represent SEM of $n = 3$. Data were normalised to the end point soluble protein concentration at the highest denaturant concentration.

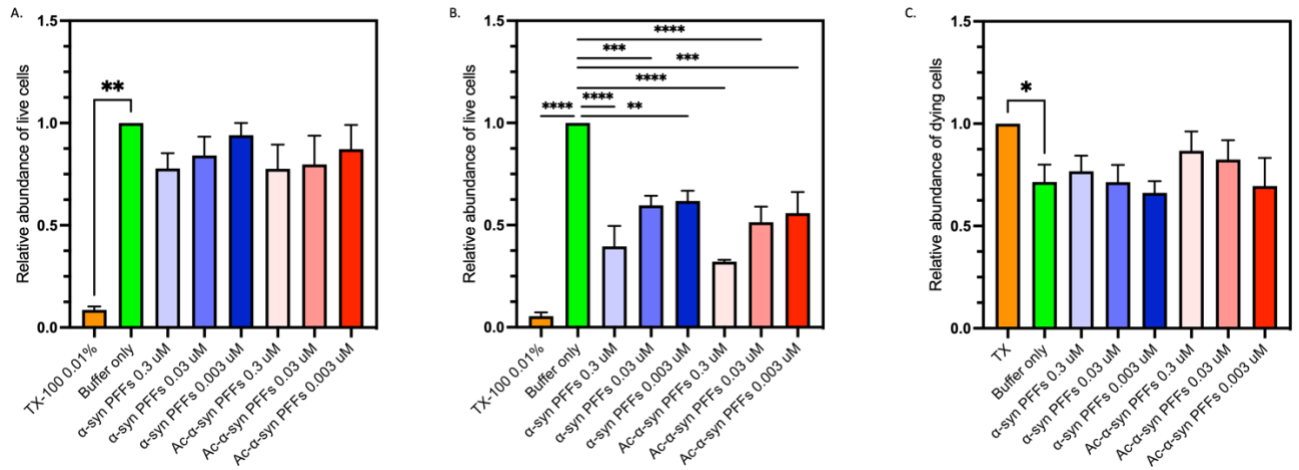


Figure 8. The N-terminal acetylation does not modify the cytotoxicity of α -synuclein fibrils and fibril fragments. (A, B) Relative end-point fluorescence intensity of Calcein AM, a live cell dye expressed in arbitrary fluorescence units, in the presence of Triton X-100 (orange), PBS (green) or when incubated with at 0.3 μ M - 0.003 μ M sonicated fibrils (PFFs) of non-acetylated α -synuclein (blue) and acetylated (Ac) α -synuclein (red) for (A) 24 h and (B) 48 h. (A) all treatments, showed significantly different fluorescence levels to Triton-X 100 treated cells ($p < 0.05$). However, a significant difference was not found between any other treatments ($p > 0.05$). (B) all treatments, showed significantly different fluorescence levels to buffer only treated control cells ($p < 0.05$). However, a significant difference was not found between acetylated and non-acetylated preformed sonicated fibrils (PFF) treatments ($p > 0.05$). (C) Relative fluorescence intensity of Propidium Iodide (PI) expressed in arbitrary fluorescence units, a dead cell detecting dye, in the presence of Triton X-100 (orange), PBS (green) or when incubated with at 0.3 μ M - 0.003 μ M sonicated fibrils (PFFs) formed from non-acetylated α -synuclein (blue) and acetylated (Ac) α -synuclein (red) for 24 h. * indicates a p value of 0.01, other pairwise comparisons showed no significant differences ($p > 0.05$).

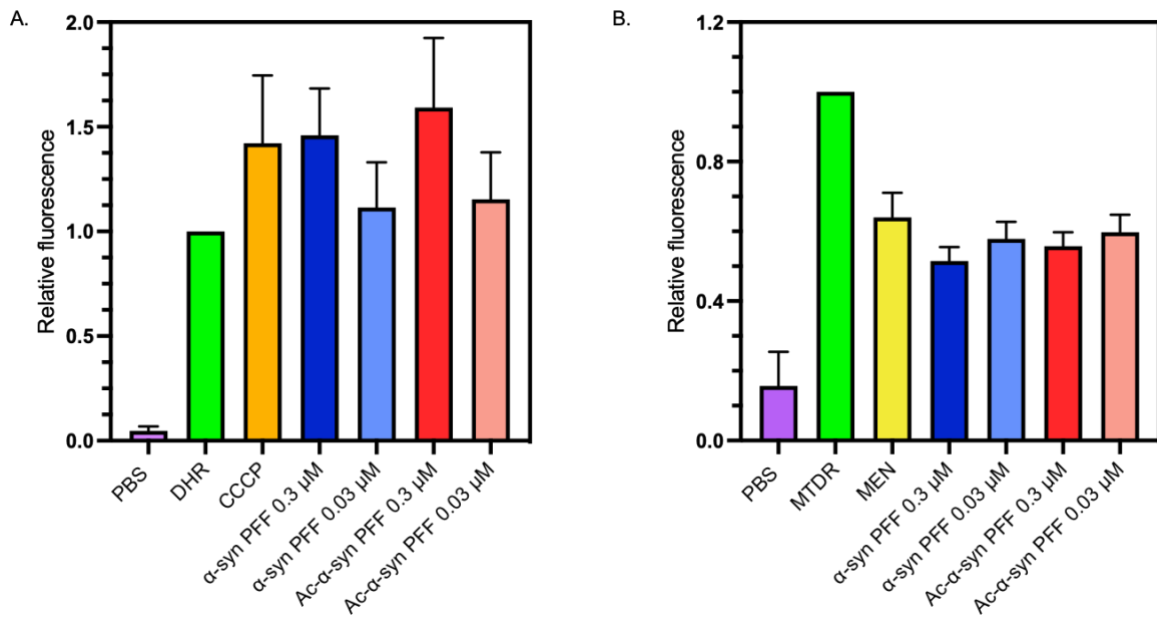


Figure 9. Comparison of the levels of reactive oxygen species (ROS) in the presence of fibrils and fibril fragments formed by non-acetylated and acetylated α -synuclein. (A) Median end-point DHR relative fluorescence intensity (B) Median end-point MTDR relative fluorescence intensity (A & B) when incubated with 0.3 μ M or 0.03 μ M of sonicated fibrils (PFFs) formed from non-acetylated- α -synuclein (blue) and acetylated- α -synuclein (red) for 30 min, or with carbonyl cyanide 3-chlorophenylhydrazone (CCCP, orange) an inducer of oxidative stress, menadione (MEN, yellow) a mitochondrial membrane potential decreasing agent for 30 min. Relative fluorescence is expressed in arbitrary fluorescence units. (A) All treatments were significantly different from DHR only (p values < 0.03), (B) all treatments were significantly different from MTDR only (p values < 0.0001) However no significant difference were found between acetylated and non-acetylated PFF treatments in A & B (p > 0.05). For both, error bars represent SEM for n = 3.

References

- (1) Simon, D. K., Tanner, C. M., and Brundin, P. (2020) Parkinson Disease Epidemiology, Pathology, Genetics, and Pathophysiology. *Clin. Geriatr. Med.* 36, 1–12.
- (2) Ray Dorsey, E., Elbaz, A., Nichols, E., Abd-Allah, F., Abdelalim, A., Adsuar, J. C., Ansha, M. G., Brayne, C., Choi, J. Y. J., Collado-Mateo, D., Dahodwala, N., Do, H. P., Edessa, D., Endres, M., Fereshtehnejad, S. M., Foreman, K. J., Gankpe, F. G., Gupta, R., Hankey, G. J., Hay, S. I., Hegazy, M. I., Hibstu, D. T., Kasaeian, A., Khader, Y., Khalil, I., Khang, Y. H., Kim, Y. J., Kokubo, Y., Logroscino, G., Massano, J., Ibrahim, N. M., Mohammed, M. A., Mohammadi, A., Moradi-Lakeh, M., Naghavi, M., Nguyen, B. T., Nirayo, Y. L., Ogbo, F. A., Owolabi, M. O., Pereira, D. M., Postma, M. J., Qorbani, M., Rahman, M. A., Roba, K. T., Safari, H., Safiri, S., Satpathy, M., Sawhney, M., Shafieesabet, A., Shiferaw, M. S., Smith, M., Szoeki, C. E. I., Tabarés-Seisdedos, R., Truong, N. T., Ukwaja, K. N., Venketasubramanian, N., Villafaina, S., Weldegewergs, K. G., Westerman, R., Wijeratne, T., Winkler, A. S., Xuan, B. T., Yonemoto, N., Feigin, V. L., Vos, T., and Murray, C. J. L. (2018) Global, regional, and national burden of Parkinson's disease, 1990–2016: a systematic analysis for the Global Burden of Disease Study 2016. *Lancet Neurol.* 17, 939–953.
- (3) Ferreira, M., and Massano, J. (2017) An updated review of Parkinson's disease genetics and clinicopathological correlations. *Acta Neurol. Scand.* 135, 273–284.
- (4) Deng, H., Wang, P., and Jankovic, J. (2018) The genetics of Parkinson disease. *Ageing Res. Rev.* 42, 72–85.
- (5) Spillantini, M. G., Schmidt, M. L., Lee, V. M., Trojanowski, J. Q., Jakes, R., and Goedert, M. (1997) α -Synuclein in Lewy bodies. *Nature* 388, 839–840.
- (6) Shahmoradian, S. H., Lewis, A. J., Genoud, C., Hench, J., Moors, T. E., Navarro, P. P., Castaño-Díez, D., Schweighauser, G., Graff-Meyer, A., Goldie, K. N., Sütterlin, R., Huisman, E., Ingrassia, A., Gier, Y. de, Rozemuller, A. J. M., Wang, J., Paepe, A. De, Erny, J., Staempfli, A., Hoernschemeyer, J., Großerüschkamp, F., Niedieker, D., El-Mashtoly, S. F., Quadri, M., Van IJcken, W. F. J., Bonifati, V., Gerwert, K., Bohrmann, B., Frank, S., Britschgi, M., Stahlberg, H., Van de Berg, W. D. J., and Lauer, M. E. (2019) Lewy pathology in Parkinson's disease consists of crowded organelles and lipid membranes. *Nat. Neurosci.* 22, 1099–1109.
- (7) Singleton, A. B., Farrer, M., Johnson, J., Singleton, A., Hague, S., Kachergus, J., Hulihan,

- M., Peuralinna, T., Dutra, A., Nussbaum, R., Lincoln, S., Crawley, A., Hanson, M., Maraganore, D., Adler, C. H., Cookson, M. R., Muentner, M., Baptista, M. J., Miller, D., Blancato, J., Hardy, J., and Gwinn-Hardy, K. (2003) α -Synuclein Locus Triplication Causes Parkinson's Disease. *Science* (80-.). 302, 841.
- (8) Chartier-Harlin, M.-C., Kachergus, J., Roumier, C., Mouroux, V., Douay, X., Lincoln, S., Levecque, C., Larvor, L., Andrieux, J., Hulihan, M., Waucquier, N., Defebvre, L., Amouyel, P., Farrer, M., and Destée, A. (2004) α -synuclein locus duplication as a cause of familial Parkinson's disease. *Lancet* 364, 1167–1169.
- (9) Zarranz, J. J., Alegre, J., Gómez-Esteban, J. C., Lezcano, E., Ros, R., Ampuero, I., Vidal, L., Hoenicka, J., Rodriguez, O., Atarés, B., Llorens, V., Gomez Tortosa, E., Del Ser, T., Muñoz, D. G., and De Yebenes, J. G. (2004) The New Mutation, E46K, of α -Synuclein Causes Parkinson and Lewy Body Dementia. *Ann. Neurol.* 55, 164–173.
- (10) Proukakis, C., Dudzik, C. G., Brier, T., MacKay, D. S., Cooper, J. M., Millhauser, G. L., Houlden, H., and Schapira, A. H. (2013) A novel α -synuclein missense mutation in Parkinson disease. *Neurology* 80, 1062–1064.
- (11) Lesage, S., Anheim, M., Letournel, F., Bousset, L., Honoré, A., Rozas, N., Pieri, L., Madiona, K., Dürr, A., Melki, R., Verny, C., and Brice, A. (2013) G51D α -synuclein mutation causes a novel Parkinsonian-pyramidal syndrome. *Ann. Neurol.* 73, 459–471.
- (12) Pasanen, P., Myllykangas, L., Siitonen, M., Raunio, A., Kaakkola, S., Lyytinen, J., Tienari, P. J., Pöyhönen, M., and Paetau, A. (2014) A novel α -synuclein mutation A53E associated with atypical multiple system atrophy and Parkinson's disease-type pathology. *Neurobiol. Aging* 35, 2180.e1-2180.e5.
- (13) Krüger, R., Kuhn, W., Müller, T., Woitalla, D., Graeber, M., Kösel, S., Przuntek, H., Eppelen, J. T., Schöls, L., and Riess, O. (1998) Ala30Pro mutation in the gene encoding α -synuclein in Parkinson's disease. *Nat. Genet.* 18, 106–108.
- (14) Polymeropoulos, M. H., Lavedan, C., Leroy, E., Ide, S. E., Dehejia, A., Dutra, A., Pike, B., Root, H., Rubenstein, J., Boyer, R., Stenroos, E. S., Chandrasekharappa, S., Athanassiadou, A., Papapetropoulos, T., Johnson, W. G., Lazzarini, A. M., Duvoisin, R. C., Di Iorio, G., Golbe, L. I., and Nussbaum, R. L. (1997) Mutation in the α -synuclein gene identified in families with Parkinson's disease. *Science* (80-.). 276, 2045–2047.
- (15) Burré, J., Sharma, M., and Südhof, T. C. T. C. (2018) Cell biology and pathophysiology of α -synuclein. *Cold Spring Harb. Perspect. Med.* 8, a024091.
- (16) Fusco, G., Pape, T., Stephens, A. D., Mahou, P., Costa, A. R., Kaminski, C. F., Kaminski Schierle, G. S., Vendruscolo, M., Veglia, G., Dobson, C. M., and De Simone, A.

- (2016) Structural basis of synaptic vesicle assembly promoted by α -synuclein. *Nat. Commun.* 7, 1–12.
- (17) Chiti, F., and Dobson, C. M. (2017) Protein Misfolding, Amyloid Formation, and Human Disease: A Summary of Progress Over the Last Decade. *Annu. Rev. Biochem.* 86, 27–68.
- (18) Fusco, G., Chen, S. W., Williamson, P. T. F., Cascella, R., Perni, M., Jarvis, J. A., Cecchi, C., Vendruscolo, M., Chiti, F., Cremades, N., Ying, L., Dobson, C. M., and De Simone, A. (2017) Structural basis of membrane disruption and cellular toxicity by alpha-synuclein oligomers. *Science* (80-.). 358, 1440–1443.
- (19) Winner, B., Jappelli, R., Maji, S. K., Desplats, P. A., Boyer, L., Aigner, S., Hetzer, C., Loher, T., Vilar, M., Campioni, S., Tzitzilonis, C., Soragni, A., Jessberger, S., Mira, H., Consiglio, A., Pham, E., Masliah, E., Gage, F. H., and Riek, R. (2011) In vivo demonstration that α -synuclein oligomers are toxic. *Proc. Natl. Acad. Sci. U. S. A.* 108, 4194–4199.
- (20) Barrett, P. J., and Timothy Greenamyre, J. (2015) Post-translational modification of α -synuclein in Parkinson's disease. *Brain Res.* 1628, 247–253.
- (21) Bell, R., and Vendruscolo, M. (2021) Modulation of the interaction between α -synuclein and lipid membranes by post-translational modifications. *Front. Neurol.* 12, 956.
- (22) Anderson, J. P., Walker, D. E., Goldstein, J. M., De Laat, R., Banducci, K., Caccavello, R. J., Barbour, R., Huang, J., Kling, K., Lee, M., Diep, L., Keim, P. S., Shen, X., Chataway, T., Schlossmacher, M. G., Seubert, P., Schenk, D., Sinha, S., Gai, W. P., and Chilcote, T. J. (2006) Phosphorylation of Ser-129 is the dominant pathological modification of α -synuclein in familial and sporadic lewy body disease. *J. Biol. Chem.* 281, 29739–29752.
- (23) Aksnes, H., Drazic, A., Marie, M., and Arnesen, T. (2016) First Things First: Vital Protein Marks by N-Terminal Acetyltransferases. *Trends Biochem. Sci.* 41, 746–760.
- (24) Johnson, M., Coulton, A. T., Geeves, M. A., and Mulvihill, D. P. (2010) Targeted amino-terminal acetylation of recombinant proteins in *E. coli*. *PLoS One* 5, 1–5.
- (25) Eastwood, T. A., and Mulvihill, D. P. (2019) Recombinant Expression and Purification of N-Acetylated Alpha-Synuclein *1856*, 113–121.
- (26) Theillet, F. X. F. X., Binolfi, A., Bekei, B., Martorana, A., Rose, H. M. H. M., Stuiver, M., Verzini, S., Lorenz, D., Van Rossum, M., Goldfarb, D., and Selenko, P. (2016) Structural disorder of monomeric α -synuclein persists in mammalian cells. *Nature* 530, 45–50.
- (27) Dedmon, M. M., Lindorff-Larsen, K., Christodoulou, J., Vendruscolo, M., and Dobson, C. M. (2005) Mapping long-range interactions in α -synuclein using spin-label NMR and ensemble molecular dynamics simulations. *J. Am. Chem. Soc.* 127, 476–477.

- (28) Sormanni, P., Aprile, F. A., and Vendruscolo, M. (2015) The CamSol method of rational design of protein mutants with enhanced solubility. *J. Mol. Biol.* 427, 478–490.
- (29) Ruzafa, D., Hernandez-Gomez, Y. S., Bisello, G., Broersen, K., Morel, B., and Conejero-Lara, F. (2017) The influence of N-terminal acetylation on micelle-induced conformational changes and aggregation of α -Synuclein. *PLoS One* 12, 1–24.
- (30) Kang, L., Janowska, M. K., Moriarty, G. M., and Baum, J. (2013) Mechanistic Insight into the Relationship between N-Terminal Acetylation of α -Synuclein and Fibril Formation Rates by NMR and Fluorescence. *PLoS One* 8, 1–10.
- (31) Bu, B., Tong, X., Li, D., Hu, Y., He, W., Zhao, C., Hu, R., Li, X., Shao, Y., Liu, C., Zhao, Q., Ji, B., and Diao, J. (2017) N-Terminal Acetylation Preserves α -Synuclein from Oligomerization by Blocking Intermolecular Hydrogen Bonds. *ACS Chem. Neurosci.* 8, 2145–2151.
- (32) Kang, L., Moriarty, G. M., Woods, L. A., Ashcroft, A. E., Radford, S. E., and Baum, J. (2012) N-terminal acetylation of α -synuclein induces increased transient helical propensity and decreased aggregation rates in the intrinsically disordered monomer. *Protein Sci.* 21, 911–917.
- (33) Maltsev, A. S., Ying, J., and Bax, A. (2012) Impact of N-terminal acetylation of α -synuclein on its random coil and lipid binding properties. *Biochemistry* 51, 5004–5013.
- (34) Bartels, T., Kim, N. C., Luth, E. S., and Selkoe, D. J. (2014) N-alpha-acetylation of α -synuclein increases its helical folding propensity, GM1 binding specificity and resistance to aggregation. *PLoS One* 9, 1–10.
- (35) Dikiy, I., and Eliezer, D. (2014) N-terminal Acetylation stabilizes N-terminal Helicity in Lipid- and Micelle-bound α -Synuclein and increases its affinity for Physiological Membranes. *J. Biol. Chem.* 289, 3652–3665.
- (36) O’Leary, E. I., Jiang, Z., Strub, M. P., and Lee, J. C. (2018) Effects of phosphatidylcholine membrane fluidity on the conformation and aggregation of N-terminally acetylated α -Synuclein. *J. Biol. Chem.* 293, 11195–11205.
- (37) Runfola, M., De Simone, A., Vendruscolo, M., Dobson, C. M., and Fusco, G. (2020) The N-terminal Acetylation of α -Synuclein Changes the Affinity for Lipid Membranes but not the Structural Properties of the Bound State. *Sci. Rep.* 10.
- (38) Iyer, A., Roeters, S. J., Schilderink, N., Hommersom, B., Heeren, R. M. A., Woutersen, S., Claessens, M. M. A. E., and Subramaniam, V. (2016) The impact of N-terminal acetylation of α -synuclein on phospholipid membrane binding and fibril structure. *J. Biol. Chem.* 291, 21110–21122.

- (39) Buell, A. K., Galvagnion, C., Gaspar, R., Sparr, E., Vendruscolo, M., Knowles, T. P. J., Linse, S., and Dobson, C. M. (2014) Solution conditions determine the relative importance of nucleation and growth processes in α -synuclein aggregation. *Proc. Natl. Acad. Sci. U. S. A.* *111*, 7671–7676.
- (40) Staats, R., Michaels, T. C. T., Flagmeier, P., Chia, S., Horne, R. I., Habchi, J., Linse, S., Knowles, T. P. J., Dobson, C. M., and Vendruscolo, M. (2020) Screening of small molecules using the inhibition of oligomer formation in α -synuclein aggregation as a selection parameter. *Commun. Chem.* *3*, 1–9.
- (41) Galvagnion, C., Buell, A. K., Meisl, G., Michaels, T. C. T., Vendruscolo, M., Knowles, T. P. J., and Dobson, C. M. (2015) Lipid vesicles trigger α -synuclein aggregation by stimulating primary nucleation. *Nat. Chem. Biol.* *11*, 229–234.
- (42) Gaspar, R., Meisl, G., Buell, A. K., Young, L., Kaminski, C. F., Knowles, T. P. J., Sparr, E., and Linse, S. (2017) Secondary nucleation of monomers on fibril surface dominates α -synuclein aggregation and provides autocatalytic amyloid amplification. *Q. Rev. Biophys.* *50*.
- (43) Fusco, G., De Simone, A., Gopinath, T., Vostrikov, V., Vendruscolo, M., Dobson, C. M., and Veglia, G. (2014) Direct observation of the three regions in α -synuclein that determine its membrane-bound behaviour. *Nat. Commun.* *5*.
- (44) Flagmeier, P., Meisl, G., Vendruscolo, M., Knowles, T. P. J., Dobson, C. M., Buell, A. K., and Galvagnion, C. (2016) Mutations associated with familial Parkinson's disease alter the initiation and amplification steps of α -synuclein aggregation. *Proc. Natl. Acad. Sci.* *113*, 10328–10333.
- (45) Brown, J. W. P., Meisl, G., Knowles, T. P. J., Buell, A. K., Dobson, C. M., and Galvagnion, C. (2018) Kinetic barriers to α -synuclein protofilament formation and conversion into mature fibrils. *Chem. Commun.* *54*, 7854–7857.
- (46) Birol, M., Wojcik, S. P., Miranker, A. D., and Rhoades, E. (2019) Identification of N-linked glycans as specific mediators of neuronal uptake of acetylated α -Synuclein. *PLoS Biol.* (Bates, G. P., Ed.) *17*, e3000318.
- (47) Yang, X., Wang, B., Hoop, C. L., Williams, J. K., and Baum, J. (2021) NMR unveils an N-terminal interaction interface on acetylated- α -synuclein monomers for recruitment to fibrils. *Proc. Natl. Acad. Sci.* *118*, e2017452118.
- (48) Burtscher, J., and Millet, G. P. (2021) Hypoxia, Acidification and Inflammation: Partners in Crime in Parkinson's Disease Pathogenesis? *Immuno* *1*, 78–90.
- (49) Guerrero-Ferreira, R., Taylor, N. M. I., Mona, D., Ringler, P., Lauer, M. E., Riek, R., Britschgi, M., and Stahlberg, H. (2018) Cryo-EM structure of alpha-synuclein fibrils. *Elife* *7*,

1–18.

(50) Buell, A. K., Dhulesia, A., White, D. A., Knowles, T. P. J., Dobson, C. M., and Welland, M. E. (2012) Detailed analysis of the energy barriers for amyloid fibril growth. *Angew. Chemie - Int. Ed.* 51, 5247–5251.

(51) Watson, M. D., and Lee, J. C. (2019) N-Terminal Acetylation Affects α -Synuclein Fibril Polymorphism. *Biochemistry* 58, 3630–3633.

(52) Chen, S. W., and Cremades, N. (2018) Preparation of α -Synuclein Amyloid Assemblies for Toxicity Experiments. *Amyloid Proteins. Methods Mol. Biol.* 1779.

(53) Guerrero-Ferreira, R., Kovacic, L., Ni, D., and Stahlberg, H. (2020) New insights on the structure of alpha-synuclein fibrils using cryo-electron microscopy. *Curr. Opin. Neurobiol.* 61, 89–95.

(54) Li, Y., Zhao, C., Luo, F., Liu, Z., Gui, X., Luo, Z., Zhang, X., Li, D., and Liu, C. (2018) Amyloid fibril structure of α -synuclein determined by cryo- electron microscopy. *Cell Res.* 1.

(55) Brás, I. C., Xylaki, M., and Outeiro, T. F. (2020) Mechanisms of alpha-synuclein toxicity: An update and outlook. *Prog. Brain Res.* 252, 91–129.

(56) Musteikytė, G., Jayaram, A. K., Xu, C. K., Vendruscolo, M., Krainer, G., and Knowles, T. P. J. (2021) Interactions of α -synuclein oligomers with lipid membranes. *Biochim. Biophys. Acta - Biomembr.* 1863, 183536.

(57) Cascella, R., Chen, S. W., Bigi, A., Camino, J. D., Xu, C. K., Dobson, C. M., Chiti, F., Cremades, N., and Cecchi, C. (2021) The release of toxic oligomers from α -synuclein fibrils induces dysfunction in neuronal cells. *Nat. Commun.* 12.

(58) Lam, H. T., Graber, M. C., Gentry, K. A., and Bieschke, J. (2016) Stabilization of α -Synuclein Fibril Clusters Prevents Fragmentation and Reduces Seeding Activity and Toxicity. *Biochemistry* 55, 675–685.

(59) Weston, S. A., and Parish, C. R. (1990) New fluorescent dyes for lymphocyte migration studies. Analysis by flow cytometry and fluorescence microscopy. *J. Immunol. Methods* 133, 87–97.

(60) Tanke, H. J., Van der Linden, P.-W. G., and Langerak, J. (1982) Alternative fluorochromes to ethidium bromide for automated read out of cytotoxicity tests. *J. Immunol. Methods* 52, 91–96.

(61) Jones, K. H., and Senft, J. A. (1985) An improved method to determine cell viability by simultaneous staining with fluorescein diacetate-propidium iodide. *J. Histochem. Cytochem.* 33, 77–79.

- (62) Fauvet, B., Fares, M. B., Samuel, F., Dikiy, I., Tandon, A., Eliezer, D., and Lashuel, H. A. (2012) Characterization of semisynthetic and naturally N α - acetylated α -synuclein in vitro and in intact cells: Implications for aggregation and cellular properties of α -synuclein. *J. Biol. Chem.* 287, 28243–28262.
- (63) Sanderson, J. B., De, S., Jiang, H., Rovere, M., Jin, M., Zaccagnini, L., Hays Watson, A., De Boni, L., Lagomarsino, V. N., Young-Pearse, T. L., Liu, X., Pochapsky, T. C., Hyman, B. T., Dickson, D. W., Klenerman, D., Selkoe, D. J., and Bartels, T. (2020) Analysis of α -synuclein species enriched from cerebral cortex of humans with sporadic dementia with Lewy bodies. *Brain Commun.* 2.
- (64) Kulenkampff, K., Wolf Perez, A. M., Sormanni, P., Habchi, J., and Vendruscolo, M. (2021) Quantifying misfolded protein oligomers as drug targets and biomarkers in Alzheimer and Parkinson diseases. *Nat. Rev. Chem.* 5, 277–294.
- (65) Hoyer, W., Antony, T., Cherny, D., Heim, G., Jovin, T. M., and Subramaniam, V. (2002) Dependence of α -synuclein aggregate morphology on solution conditions. *J. Mol. Biol.* 322, 383–393.
- (66) Weinreb, P. H., Zhen, W., Poon, A. W., Conway, K. A., and Lansbury, P. T. (1996) NACP, a protein implicated in Alzheimer's disease and learning, is natively unfolded. *Biochemistry* 35, 13709–13715.
- (67) Micsonai, A., Wien, F., Bulyáki, É., Kun, J., Moussong, É., Lee, Y. H., Goto, Y., Réfrégiers, M., and Kardos, J. (2018) BeStSel: A web server for accurate protein secondary structure prediction and fold recognition from the circular dichroism spectra. *Nucleic Acids Res.* 46, W315–W322.
- (68) Olsson, M., Wilson, M., Uller, T., Mott, B., and Isaksson, C. (2009) Variation in levels of reactive oxygen species is explained by maternal identity, sex and body-size-corrected clutch size in a lizard. *Naturwissenschaften* 96, 25–29.
- (69) Felle, H., and Bentrup, F. W. (1977) A study of the primary effect of the uncoupler carbonyl cyanide m-chlorophenylhydrazone on membrane potential and conductance in *Riccia fluitans*. *BBA - Biomembr.* 464, 179–187.
- (70) Loor, G., Kondapalli, J., Schriewer, J. M., Chandel, N. S., Vanden Hoek, T. L., and Schumacker, P. T. (2010) Menadione triggers cell death through ROS-dependent mechanisms involving PARP activation without requiring apoptosis. *Free Radic. Biol. Med.* 49, 1925–1936.
- (71) Robinson, K. M., Janes, M. S., Pehar, M., Monette, J. S., Ross, M. F., Hagen, T. M., Murphy, M. P., and Beckman, J. S. (2006) Selective fluorescent imaging of superoxide in

vivo using ethidium-based probes. *Proc. Natl. Acad. Sci. U. S. A.* 103, 15038–15043.

(72) Xiao, B., Deng, X., Zhou, W., and Tan, E. K. (2016) Flow cytometry-based assessment of mitophagy using mitotracker. *Front. Cell. Neurosci.* 10, 76.

(73) Galvagnion, C. (2017) The Role of Lipids Interacting with α -Synuclein in the Pathogenesis of Parkinson's Disease. *J. Parkinsons. Dis.* 7, 433–450.

(74) Dear, A. J., Michaels, T. C. T., Meisl, G., Klenerman, D., Wu, S., Perrett, S., Linse, S., Dobson, C. M., and Knowles, T. P. J. (2020) Kinetic diversity of amyloid oligomers. *Proc. Natl. Acad. Sci. U. S. A.* 117.

(75) Fanning, S., Selkoe, D., and Dettmer, U. (2020) Parkinson's disease: proteinopathy or lipidopathy? *NPJ Park. Dis.* 6, 3.